

# *More-persistent weak stratospheric polar vortex states linked to cold extremes*

Article

Accepted Version

Kretschmer, M. ORCID: <https://orcid.org/0000-0002-2756-9526>, Coumou, D., Agel, L., Barlow, M., Tziperman, E. and Cohen, J. (2018) More-persistent weak stratospheric polar vortex states linked to cold extremes. *Bulletin of the American Meteorological Society*, 99 (1). pp. 49-60. ISSN 1520-0477 doi: <https://doi.org/10.1175/BAMS-D-16-0259.1> Available at <https://centaur.reading.ac.uk/92432/>

It is advisable to refer to the publisher's version if you intend to cite from the work. See [Guidance on citing](#).

Published version at: <http://dx.doi.org/10.1175/BAMS-D-16-0259.1>

To link to this article DOI: <http://dx.doi.org/10.1175/BAMS-D-16-0259.1>

Publisher: American Meteorological Society

All outputs in CentAUR are protected by Intellectual Property Rights law, including copyright law. Copyright and IPR is retained by the creators or other copyright holders. Terms and conditions for use of this material are defined in the [End User Agreement](#).

[www.reading.ac.uk/centaur](http://www.reading.ac.uk/centaur)

**CentAUR**

Central Archive at the University of Reading

Reading's research outputs online

# More-persistent weak stratospheric polar vortex states linked to cold extremes

## Authors

Marlene Kretschmer<sup>\*1,2</sup>, Dim Coumou<sup>1,3</sup>, Laurie Agel<sup>4,5</sup>, Mathew Barlow<sup>4</sup>, Eli Tziperman<sup>6</sup>,  
Judah Cohen<sup>\*7</sup>

## Affiliations

<sup>1</sup>Potsdam Institute for Climate Impact Research, Earth System Analysis, Potsdam, Germany

<sup>2</sup>Department of Physics, University of Potsdam, Germany

<sup>3</sup>Institute for Environmental Studies (IVM), VU University Amsterdam

<sup>4</sup>Department of Environmental, Earth, and Atmospheric Sciences, University of

Massachusetts Lowell, Lowell, MA, USA

<sup>5</sup>Intercampus Marine Science Graduate Program, University of Massachusetts, MA, USA

<sup>6</sup>Department of Earth and Planetary Sciences and School of Engineering and Applied

Sciences, Harvard University, Cambridge, MA, USA

<sup>7</sup>Atmospheric and Environmental Research, Lexington, MA, USA

\*Corresponding authors:

kretschmer@pik-potsdam.de (M.K.), jcohen@aer.com (J.C.)

## 21 **Abstract**

22 The extra-tropical stratosphere in boreal winter is characterized by a strong circumpolar  
23 westerly jet, confining the coldest temperatures at high latitudes. The jet, referred to as the  
24 stratospheric polar vortex, is predominantly zonal and centered around the pole; however, it  
25 does exhibit large variability in wind speed and location. Previous studies showed that a  
26 weak stratospheric polar vortex can lead to cold-air outbreaks in the mid-latitudes but the  
27 exact relationships and mechanisms are unclear. Particularly, it is unclear whether  
28 stratospheric variability has contributed to the observed anomalous cooling trends in mid-  
29 latitude Eurasia. Using hierarchical clustering, we show that over the last 37 years, the  
30 frequency of weak vortex states in mid to late winter (January and February) has increased  
31 which were accompanied by subsequent cold extremes in mid-latitude Eurasia. For this  
32 region 60% of the observed cooling in the era of Arctic amplification, i.e. since 1990, can be  
33 explained by the increased frequency of weak stratospheric polar vortex states, a number  
34 which increases to almost 80% when El Niño/Southern Oscillation (ENSO) variability is  
35 included as well.

36

37

## 38 **Capsule**

39 Over the last decades, the stratospheric polar vortex has shifted towards more frequent  
40 weak states which can explain Eurasian cooling trends in boreal winter in the era of Arctic  
41 amplification.

## 42 **Introduction**

43 Despite global warming, recent winters in the Northeastern United States (US), Europe and  
44 especially in Asia were anomalously cold. Some mid-latitude regions like Central Asia and  
45 eastern Siberia even show a downward temperature trend in winter over the past decades  
46 (Cohen et al. 2014a; McCusker et al. 2016). In contrast, the Arctic has been warming rapidly,  
47 challenging scientists to explain the so called warm Arctic – cold continents pattern in boreal  
48 winter (Shepherd 2016). Though there is general agreement that sea ice loss contributed to  
49 the warming of the Arctic via ice-albedo feedbacks (Screen and Simmonds 2010), it remains  
50 controversial whether observed mid-latitude cooling is related to internal atmospheric  
51 variability (Sun et al. 2016; McCusker et al. 2016), to tropical (Palmer 2014) or Arctic (Cohen  
52 et al. 2013; Cohen 2016) trends in teleconnection indices, or a combination of those.

53 Previous research showed that a weak stratospheric polar vortex (hereafter also referred to  
54 as ‘polar vortex’ or ‘vortex’) can affect surface weather via a downward influence of  
55 planetary waves (Baldwin and Dunkerton 2001; Hitchcock and Simpson 2014) which leads to  
56 cold air outbreaks in the mid-latitudes and a negative surface Arctic Oscillation signal (Cohen  
57 et al. 2013; Kolstad et al. 2010; Butler et al. 2014; Baldwin and Dunkerton 2001; Sigmond et  
58 al. 2013; Kretschmer et al. 2016). Moreover, it was shown that Sudden Stratospheric  
59 Warmings (SSW) can modulate the tropospheric flow for up to two months (Baldwin and  
60 Dunkerton 2001; Hitchcock and Simpson 2014) which can even offset the impact of El Niño  
61 Southern Oscillation (ENSO) events (Polvani et al. 2016). Consequently, including  
62 stratosphere activity in climate models significantly improves seasonal forecast skill for  
63 winter weather (Scaife et al. 2016; Sigmond et al. 2013). Despite this key role of the polar  
64 vortex for winter circulation and surface temperature, a quantitative analysis of the  
65 potential stratospheric role for the recent cooling trends has yet been lacking.

66 There are several metrics to describe polar vortex variability, extreme states and its coupling  
67 with the troposphere but the different indices do not necessarily capture all of these  
68 aspects. Often, the stratospheric impact on surface temperatures is analyzed in the context  
69 of Sudden Stratospheric Warmings (Polvani et al. 2016; Butler et al. 2014). Detection of  
70 SSWs is, however, sensitive to their exact definition, which varies throughout the literature  
71 (Butler et al. 2015). Moreover, SSWs are individual rare events and thus do not describe the  
72 overall behavior of the vortex. The tropospheric response of SSWs depends, however, on  
73 their temporal evolution and persistence in the stratosphere (Kodera et al. 2016; Runde et  
74 al. 2016). To study the recovery phase of extreme stratospheric events, Hitchcock et al.  
75 (2013) identified polar-night jet oscillation (PJO) events. These describe long-lasting  
76 anomalous warm temperatures in the stratospheric polar cap and are often preceded by  
77 SSWs, but approximately half of the SSWs recover rapidly from the abrupt warming  
78 (Hitchcock et al. 2013b).

79 Recently, machine learning approaches such as clustering algorithms have successfully been  
80 applied to study impacts of and changes in circulation patterns (Feldstein and Lee 2014;  
81 Horton et al. 2015; Lee and Feldstein 2013; Cheng and Wallace 1993), providing a promising  
82 data-driven tool to classify atmospheric fields. Motivated by these results, we perform  
83 cluster analysis on the daily extra-tropical stratosphere to identify its dominant spatial  
84 patterns and temporal evolution. This way we can study different vortex states as well as  
85 persistence of specific events. We analyze how long-term changes in polar vortex variability  
86 might have affected surface warming patterns.

87

## 88 **Data**

89 We use daily mean ERA-Interim (Dee et al. 2011) data from January 1979 to December 2015  
90 leap days excluded. Data that were used to characterize the stratospheric polar vortex  
91 (geopotential height and zonal wind velocity at 10hPa) were provided on a  $0.75^\circ \times 0.75^\circ$   
92 latitude-longitude grid. To study precursors and lagged effects of different polar vortex  
93 cluster events, we use gridded ( $3^\circ \times 3^\circ$ ) data of sea-level pressure, near surface temperature  
94 and poleward heat-flux ( $v \cdot T^*$ ) at 100hPa, where  $v$  is the meridional wind velocity,  $T$  is the  
95 temperature and the asterisks denote the deviation from the zonal mean. We further use  
96 daily mean MERRA-2 (Molod et al. 2015) data from 1980-2015 to perform sensitivity  
97 analyses on the reanalysis product and clustering technique used.

98

## 99 **Methods**

100 We employ hierarchical clustering (Cheng and Wallace 1993) on the daily mean zonal wind  
101 velocity field poleward of  $60^\circ\text{N}$  at 10hPa. We chose this domain and level for consistency  
102 with most other SSW definitions and polar vortex studies (Butler et al. 2015). We limit the  
103 cluster analysis to the months January and February over the period 1979-2015, as these  
104 months show the strongest polar vortex variability. First we calculate the climatological  
105 anomalies for each day by subtracting their multi-year mean. Additionally, to account for the  
106 denser grid towards the pole, we apply area-weighting. There are  $n = 2183$  daily  
107 observations (37 years times 59 days), each corresponding to a vector of length 19,680  
108 (number of grid points in our domain) representing the state of the polar vortex on a  
109 particular winter day. The cluster algorithm groups days with similar extra-tropical

110 stratospheric wind fields in one cluster which can be represented by the composite of all  
111 days assigned to it (see Appendix and Supplementary Information for more details).

112 We determine time series of the seasonal occurrence frequencies for each cluster which  
113 ranges from zero (absent) to one (every day of the winter was assigned to that cluster).  
114 Linear trends in occurrence frequency are calculated using a least-square fit regression  
115 model and the slope was tested for significance using a two-sided Student's t-test. We  
116 define a cluster "event" as a period of consecutive days for which the same cluster is  
117 identified.

118

### 119 **More frequent weak polar vortex states**

120 Our analysis reveals that seven is an appropriate choice for the number of clusters, providing  
121 a sufficiently detailed overview of the spectrum of different polar vortex patterns, while still  
122 allowing each pattern to describe a significant part of the total polar vortex phase space (see  
123 Appendix and SI). This is also demonstrated by the relatively high mean pattern correlation  
124 of 0.59, which is used to estimate how well the clusters represent the original data: the  
125 area-weighted pattern correlation of each daily field to its cluster-composite is calculated,  
126 and the average over all days represents a global measure of similarity.

127 Figure 1 shows the composite mean of the 10hPa geopotential height field for all seven  
128 clusters, ordered by polar cap height (i.e. the area-weighted 10hPa geopotential heights  
129 mean north of 60°N), starting with the strongest polar vortex cluster (thus with the lowest  
130 polar cap height). Though clustering was performed on the zonal wind field, we present  
131 geopotential heights for easier visualization of the different polar vortex shapes. The  
132 associated zonal wind plots are given in Fig. S3. The patterns range from a strong



133 circumpolar vortex (cluster 1) to a slightly less-strong polar vortex (cluster 2), to  
134 progressively weaker polar vortices with displaced vortex centers towards Eurasia (cluster 3,  
135 5, 6) and North America (cluster 4) and finally a weak distorted vortex (cluster 7). Below the  
136 cluster composites, time series of their seasonal frequency with a linear least square fit  
137 trend line are displayed for each cluster. The strong vortex cluster (cluster 1) has a significant  
138 ( $P = 0.047$ ) downward linear trend of  $-0.2 (37y)^{-1}$  whereas the weak vortex clusters 5, 6 and 7  
139 increased in frequency, the last with a trend of  $0.12 (37y)^{-1}$  ( $P=0.146$ ).

140 In principle, it is possible that trends in (seasonal) frequency are only the result of two or  
141 more similar clusters with opposing trends that would cancel each other out if those clusters  
142 were merged. To test this possibility, we calculate for each day the pattern correlation with  
143 the composite mean of each cluster (Fig. S4, see SI for details). This thus quantifies how the  
144 daily polar vortex patterns resemble the different clusters at each time-step. We find that  
145 the strong vortex clusters (cluster 1, 2) exhibit a downward trend in pattern correlation  
146 ( $P \approx 0.07$ ). In contrast, the weak vortex clusters (cluster 6, 7) have upward trends ( $P \approx 0.07$ ).  
147 Thus, over the last 37 winters, the daily polar vortex state shifted towards the weaker cluster  
148 patterns. This is consistent with the overall weakening of the stratospheric zonal wind field,  
149 especially at the vortex edge over the continents (Fig. 2a, S5 for the polar cap mean). South  
150 of  $60^\circ\text{N}$  the trends in zonal wind velocity are even upward, indicating an equatorward shift  
151 and broadening in addition to the weakening of the vortex.

152 To test how well our cluster analysis reflects observed trends, we multiply the zonal wind  
153 composite mean of each cluster with the slope of its frequency trend (Lee and Feldstein  
154 2013). Summed for all clusters (Fig. 2b), this shows how much of the seasonal mean change  
155 is explained by the change in frequencies and we find that it compares well with the actual  
156 trend field (Fig. 2a). In fact, approximately 72% of the observed weakening north of  $60^\circ\text{N}$  is

157 already explained by the less frequent occurrence of the strong vortex cluster 1 and the  
158 more frequent occurrence of the weak polar vortex cluster 7 (Fig. 2c).

159 To further test how the frequency of cluster events changes over time, we count the mean  
160 seasonal occurrence in the first half (1979-1996) and the second half (1998-2015) of the  
161 studied time-period for each cluster (Fig. 3a). We find that the frequency of cluster 7  
162 increased significantly (using a bootstrapping approach; see Appendix) by 140% from on  
163 average ca. 3 days per winter up to roughly 7 days ( $P < 0.01$ ). In contrast, the frequency of  
164 cluster 1 halved from approximately 12 days per season to just 6 ( $P < 0.05$ ). The increased  
165 frequency of cluster 7 days results from an increase in the persistence of cluster 7 events  
166 (consecutive days assigned to cluster 7). Whereas in the first half of the studied time-period  
167 the mean persistence of cluster 7 events was 5.3 days, it was significantly ( $P < 0.01$ ) longer in  
168 the second half with events persisting on average 14.1 days (an increase by more than  
169 160%). In contrast, the mean persistence of cluster 1 events was approximately 9 days in  
170 both periods, but their occurrence dropped notably from 27 events in the first half to just 11  
171 events in the latter half. Thus, the increase in cluster 7 days is due to longer events and the  
172 decrease in cluster 1 days is due to less events.

173

## 174 **Robust classification of weak polar vortex states**

175 Our finding of more (less) frequent weak (strong) polar vortex days over the past winters is  
176 robust and insensitive to the total number of clusters (from 2 to 20 clusters). Furthermore,  
177 the cluster representatives and frequency trends of the strongest and the weakest cluster  
178 are robustly identified and are mostly insensitive to the data-set (MERRA-2 instead of ERA-  
179 Interim), clustering technique (using k-means or self-organizing maps instead of hierarchical

180 clustering), clustered variable (geopotential heights instead of zonal wind velocity) and  
181 pressure level (100hPa and the mean over 10-50hPa). Generally, clustering over lower  
182 pressure levels results in higher seasonal frequencies of weak polar vortex states. This is  
183 consistent with previous studies showing that disturbances of the upper stratospheric flow  
184 persist for longer when they descend to lower levels (Hitchcock et al. 2013b,a) and also with  
185 the fact that strong lower-stratospheric anomalies often coincide with tropospheric  
186 circulation anomalies (Baldwin and Dunkerton 2001) which, are not necessarily observed at  
187 higher levels. More precise information how the different tests compare can be found in the  
188 Supplementary Information (Fig. S6-S15).

189 Our clustering methodology is also consistent with other metrics to classify extremely weak  
190 states of the stratospheric polar vortex. All starting days of major SSWs in January and  
191 February, as detected by Charlton and Polvani (2007), are assigned to the weak vortex  
192 clusters 6 and 7 (Fig. S17), which also coincide with polar-night oscillation events (Fig. S16,  
193 Hitchcock et al. 2013b). In summary, the different sensitivity tests show that a cluster  
194 approach applied at 10hPa provides a robust and appropriate methodology to study the  
195 occurrence and persistence of weak polar vortex events as well as their coupling with lower  
196 stratospheric pressure levels.

197

## 198 **Links to surface temperature**

199 The tropospheric response to weak polar vortex states can influence surface weather for up  
200 to two months (Baldwin and Dunkerton 2001; Hitchcock and Simpson 2014; Sigmond et al.  
201 2013). Further, the tropospheric response is more pronounced if the stratospheric recovery  
202 is slow following a vortex disturbance (Kodera et al. 2016; Runde et al. 2016). Thus, an

203 increase in more persistent weak polar vortex states, i.e. longer-lived cluster 7 events, could  
204 potentially influence winter temperatures. In other words, the moderate changes in the  
205 mean vortex state (Fig. S5) are much less relevant for surface conditions than the increased  
206 persistence of extremely weak states.

207 To study the relationship of cluster 1 and 7 events with surface weather, we create  
208 composites of (detrended) near-surface temperature (Fig. 4). As expected, strong vortex  
209 states (cluster 1) coincide with mild temperatures in the Eastern US and Northern Eurasia  
210 and cold temperatures over Alaska and Greenland (Fig. 4a). In contrast, during weak vortex  
211 states (cluster 7), anomalously cold temperatures are observed in Northern Eurasia whereas  
212 Canada is anomalously warm (Fig. 4b). Thus, the increased frequency in cluster 7 during  
213 recent winters might be linked to the surface cooling trends over Eurasia. To test this, we  
214 first determine different linear regression models onto mean winter (JF) near-surface  
215 temperature at each grid-point and plot their  $R^2$  values (Fig. 5), indicating how much of the  
216 observed temperature variability is explained by the linear model. To account for potential  
217 biases due to trends in the regressors and the temperature time-series, we detrended the  
218 variables first. Though polar cap height (PCH) variability can explain already some seasonal  
219 temperature variability (Fig. 5b), regression by cluster 7 seasonal frequency gives higher  $R^2$   
220 values, significant over extended regions, including Central Siberia, Eastern Canada and the  
221 Western Atlantic sector but not the United States (Fig. 5c). The combination of ENSO  
222 (described by the mean winter Nino3.4 index) and the seasonal frequency of cluster 7  
223 further improves the results over the Pacific and parts of the United States (Fig. 5d) but  
224 ENSO alone has very little influence on Eurasian temperature variability (Fig. 5a). Note that  
225 the correlation between the detrended cluster 7 frequency time-series and the detrended  
226 Nino3.4 index is only 0.01, showing that they are almost completely independent.

227 Next, we calculate the temperature trends at each grid-point for each of the regression  
228 models (Fig. 6a-c). For consistency with previous studies analyzing the warm Arctic-cold  
229 continent pattern (Sun et al. 2016; Cohen et al. 2013; Cohen 2016; McCusker et al. 2016), we  
230 calculate trends over the era of Arctic amplification (Cohen et al. 2014a), i.e. from 1990  
231 onward. We apply the regression parameters from the models calculated for the detrended  
232 data from 1979-2015 (Fig. 5) to predict temperature trends using the non-detrended  
233 regressors from 1990-2015. All models show a warm Arctic - cold continent pattern, with  
234 much stronger cooling over Eurasia than over North America. The explanatory power of  
235 ENSO (Fig. 6a) and polar cap heights at 10hPa (not shown) is small. In contrast, regression by  
236 cluster 7 frequency (Fig. 6b) captures the observed Eurasian pattern well. The best  
237 agreement with observations (Fig. 6d) is achieved with the models including both cluster 7  
238 and the Nino3.4 index (Fig. 6c). Thus, although other factors certainly play a role as well, the  
239 observed cooling trends over Eurasia (Fig. 6d) are well captured by the trend towards more-  
240 persistent weak vortex states (Fig. 6b), something which can be further improved by  
241 including tropical variability (Fig. 6c).

242

## 243 **Cold weather in Eurasia**

244 Several studies focused on Eurasia as the winter cooling trend has been more pronounced  
245 (McCusker et al. 2016; Sun et al. 2016; Li et al. 2015; Mori et al. 2014). Indeed, our analyses  
246 show that the relationship between weak polar vortex states and surface temperature is  
247 much stronger for this region, as compared to the northeastern US (Fig. 4b, 5c, 6b).

248 Our predicted regression model based on cluster 7 correlates ( $r = 0.46$ ,  $R^2 = 0.21$ )  
249 significantly ( $P < 0.01$ , according to a Student's t-test) with winter temperature averaged over

the Eurasian sector (15°-130°E, 50°-65°N, black box in Fig. 7a). This model performs much better than a regression model based on the polar cap height (PCH) index at 10hPa ( $r = 0.26$ ,  $R^2 = 0.07$ ,  $P = 0.11$ ). Thus, the seasonal frequency of weak states is a better predictor for Eurasian temperature variability than the polar cap mean. Moreover, the cluster 7 based model explains ~60% of the domain-mean Eurasian cooling trend since 1990 (-0.95°K per decade). For ENSO and the polar cap height this is respectively only 17% and 24%. When ENSO is combined with cluster 7, the percent of the recovered cooling trend in Eurasia jumps to 77%. This shows that the trend towards more-persistent weak polar vortex states can explain most of the winter cooling trend over northern Eurasia.

Next we consider Eurasian cold extremes (defined as days when the temperature anomaly over the Eurasian sector is below  $<-5^{\circ}\text{C}$ , coinciding with the 10<sup>th</sup> percentile) and calculate the relative occurrence frequency of each cluster. For the Null-Hypothesis, i.e. that stratospheric variability plays no role, one would expect for each cluster a frequency during cold extremes approximately equal to its occurrence over all winter days as displayed in Figure 1. Though only 8.25% of all considered days were assigned to cluster 7 (Fig. 1), the likelihood of cluster 7 days roughly doubles to 17.2% if only cold days are considered (Fig. 7b), which is a significant increase ( $P < 0.01$ , according to a chi-square test). The occurrence of cluster 6 days also exceeds the expected frequency whereas the strong vortex clusters 1-3 occur less often than statistically expected. Similarly, only 3% of the hottest days (exceeding the 90<sup>th</sup> percentile) are cluster 7 days, which significantly ( $P < 0.01$ ) differs notably from the expected occurrence of ~8% (not shown).

To assess the direction of causality between weak vortex states and Eurasian cold extremes we perform lagged coincidence analysis. In the week before the onset of cluster 7 events, most days are assigned to weak polar vortex states (51% cluster 6, 20% cluster 5), which

274 themselves are already associated with low temperatures anomalies over Eurasia. The mean  
275 Eurasian temperature anomaly preceding cluster 7 events is  $-1.2^{\circ}\text{C}$  but it reaches its  
276 minimum value during cluster 7 events with an average anomaly of  $-1.9^{\circ}\text{C}$ . Thus, cluster 7  
277 days represent the peak of the polar vortex disturbance as well as the peak of the cold  
278 anomalies over the northern Eurasian sector. Consistently, in the week before the onset of a  
279 cold event, the likelihood of cluster 6 is anomalously high. If we merge cluster 6 and 7, the  
280 mean Eurasian temperature during these weak vortex states is still negative ( $-1.1^{\circ}\text{C}$ ) but the  
281 temperature in the preceding week is anomalously warm at  $+0.4^{\circ}\text{C}$ . Thus, since weak vortex  
282 events (clusters 6 and 7) are preceded by positive temperature anomalies in Eurasia, we  
283 propose that the observed cooling trend in this region is more likely the consequence of the  
284 vortex weakening rather than its cause. Moreover, we found that cluster 7 Granger causes  
285 Eurasian temperature variability in winter and that the opposite is not true, which further  
286 supports this assumption (see SI). This is also consistent with recent findings, showing that  
287 cold spells over Eurasia are longer-lasting if accompanied by a weak polar vortex (Garfinkel  
288 et al. 2017).

289

## 290 **Precursors and potential reasons for weak polar vortex states**

291 Finally, we analyze potential reasons for the observed trends in frequency of the polar  
292 vortex cluster 1 and 7. Both observational and modeling studies have shown that strong  
293 upward wave propagation in the upper troposphere can weaken the stratospheric flow  
294 (Jaiser et al. 2013; Kretschmer et al. 2016; Kim et al. 2014; Polvani and Waugh 2004; Shaw et  
295 al. 2014) as expected on theoretical grounds (Matsuno 1970) and is often preceded by  
296 distinct sea level pressure anomalies (Baldwin and Dunkerton 1999; Cohen and Jones 2011;

297 Kretschmer et al. 2016). Therefore, we created composites of anomalies in sea level pressure  
298 (30-10 days before the start date of cluster events) and meridional heat-flux  $v^*T^*$  at 100hPa  
299 (10 days prior to the cluster events), which is a common proxy for vertical wave propagation  
300 (Fig. 8a-d, showing only those for clusters 1 and 7). The choice of time-lags was motivated by  
301 previous studies (Kretschmer et al. 2016; Kim et al. 2014; Cohen and Jones 2011) but the  
302 results are also robust for time-shifts of a few days. In the month before the onset of a weak  
303 polar vortex event, sea level pressure over most of northwest Eurasia is anomalously high  
304 while sea level pressure over the Chukchi Sea, North America and the Northern Atlantic is  
305 anomalously low (Fig. 8b). This pressure dipole is followed by an anomalously strong  
306 poleward heat-flux over Northern Europe, Central Asia and Chukchi and Beaufort Seas and a  
307 lower than normal heat-flux north over the Lena river and over northern Canada (Fig. 8d). In  
308 contrast, strong polar vortex events are preceded by patterns of opposite sign of sea level  
309 pressure and heat-flux anomalies but are of less amplitude (Fig. 8a, c).

310 Vice versa, to test if high western Siberian sea level pressure events are also followed by  
311 weak polar vortex states (in a statistically significant way) we create an index of area-  
312 averaged sea level pressure over the Ural Mountains region (45-70°N, 40-85°E) for  
313 December and January (Cohen et al. 2014b; Kretschmer et al. 2016). We define strong  
314 western Siberian High events when the index exceeds 1035hPa, which corresponds to the  
315 93rd percentile. In the month following high sea level pressure over western Siberia in  
316 December and January the frequency of cluster 7 events triples (from 8.25% to 26.1%,  
317  $P < 0.01$ ) whereas that of cluster 1 events halves (from 16.12% to 7.15%,  $P < 0.01$ ; see  
318 Appendix). Thus, not only are cluster 7 events preceded by high sea level pressure over the  
319 Ural Mountains but also high sea level pressure anomalies over western Siberia strongly  
320 increase the likelihood of weak polar vortex states.



321 The cluster 7  $v^*T^*$  precursor anomalies (Fig. 8d) correspond to a reinforcement of the  
322 climatological poleward heat-flux, which has shown to lead to a weakened polar vortex  
323 (Polvani and Waugh 2004; Dunn-Sigouin and Shaw 2015; Shaw et al. 2014). Moreover, the  
324 sea level pressure composites for cluster 7 (Fig. 8b) are consistent with different studies  
325 linking increased vertical wave propagation to tropospheric forcing (Kretschmer et al. 2016;  
326 Feldstein and Lee 2014; Cohen and Jones 2011). Constructive interference with the  
327 climatological high leads to more vertical wave activity in the upper troposphere and  
328 thereby a weakening of the polar vortex (Feldstein and Lee 2014; Kretschmer et al. 2016;  
329 Cohen et al. 2014b; Smith et al. 2010). Thus, the detected precursors of cluster 7 are in  
330 accordance with known physical mechanisms of troposphere-stratosphere coupling.

331 The formation of anomalous high pressure over Northern Eurasia has been associated with  
332 late autumn Barents and Kara sea ice loss and enhanced Eurasian October snow cover extent  
333 (Kim et al. 2014; Kretschmer et al. 2016; Feldstein and Lee 2014; Cohen et al. 2014b).  
334 Therefore, we speculate that these processes, which have been linked to Arctic amplification  
335 (Cohen et al. 2014a; Overland et al. 2011) and which have also been reproduced by climate  
336 models (Jaiser et al. 2016; Handorf et al. 2015), contributed to the patterns that favor a  
337 weakened polar vortex represented by cluster 7 (Fig. 8b, d). Moreover, the involved time-lag  
338 of approximately three months (Kretschmer et al. 2016) for these Arctic driven mechanisms  
339 might explain why clustering with November and December data exhibits no trends in the  
340 frequency of the different vortex clusters (Fig. S9). The negative sea level pressure anomalies  
341 over the North Pacific for cluster 7 events (Fig. 8b) are also similar to patterns associated  
342 with El Niño years, which are associated with a weak polar vortex (Baldwin and O’Sullivan  
343 1995; Polvani et al. 2016). However, since different ENSO indices did not show any trend  
344 over the last decades, the weakening polar vortex can probably not be explained by ENSO

345 related teleconnections. Nevertheless, the interplay between different tropical  
346 teleconnections (Garfinkel and Hartmann 2008), natural variability (McCusker et al. 2016)  
347 and variability in atmospheric responses to Arctic sea ice loss (Screen and Francis 2016) as  
348 well as impacts of regional differences in sea ice decline (Sun et al. 2015) might influence the  
349 stratospheric response. This interplay of possible causal drivers requires further analyses  
350 using both climate models and observations (Overland et al. 2016).

351

## 352 **Conclusion**

353 Using cluster analysis, we identified dominant patterns of the stratospheric polar vortex in  
354 boreal winter. We showed that the polar vortex weakening over the last four decades was a  
355 result of more-persistent weak polar vortex states (cluster 7) and less frequent strong polar  
356 vortex events (cluster 1) rather than an overall weakening. This shift in polar vortex states  
357 can account for most of the recent winter cooling trends over Eurasian mid-latitudes via  
358 stratosphere-troposphere coupling. The observed sea level pressure and heat-flux  
359 precursors are in agreement with proposed physical mechanisms and can explain the  
360 weakening of the polar vortex via a dynamical troposphere-stratosphere coupling.

361 Our analysis shows that the Eurasian cooling trend in the era of Arctic amplification can  
362 largely be explained by polar vortex variability. Understanding the two-way link between  
363 stratospheric and tropospheric circulation is hence essential for understanding winter  
364 teleconnections in the northern hemisphere. Any improvements in winter-time seasonal  
365 forecasts are likely to depend on our comprehension of competing drivers including the  
366 influence of stratospheric variability (Sigmond et al. 2013; Kretschmer et al. 2016).

367

## 368 **Acknowledgements**

369 We thank Peter Hitchcock and two anonymous reviewers for their useful comments and  
370 suggestion to improve the manuscript and we thank ECMWF and GMAO for making the ERA-  
371 Interim and the MERRA-2 data available. The work was supported by the German Federal  
372 Ministry of Education and Research, grant no. 01LN1304A, (M.K., D.C.), the National Science  
373 Foundation (NSF) grants AGS-1303647 and PLR-1504361, NOAA grant NA15OAR4310077  
374 (J.C.) and grant AGS-1303604 (E.T.). The research project resulted from M.K. visiting J.C. and  
375 M.K. would like to thank AER and Harvard for hosting. E.T. would like to thank the Weizmann  
376 Institute for its hospitality during parts of this work.

377

## 378 **Appendix A: Methods**

### 379 **Clustering**

380 The hierarchical cluster algorithm starts with  $n$  clusters (the starting vectors) and then  
381 iteratively merges two clusters until only one cluster (the mean over all vectors) exists. In  
382 each step the clusters with minimal distance are merged and their mean is calculated. Here  
383 we use Ward's metric criteria, meaning that the two clusters to be merged at each step are  
384 those which result in the minimal increase in variance in the merged cluster, over all possible  
385 unions of clusters.

386 While more computationally demanding, hierarchical clustering has the advantage over  
387 other clustering techniques such as k-means or self-organizing maps (SOM), that no a-priori  
388 knowledge on the number of clusters is required. Each of the  $n-1$  merging steps can be  
389 tracked back and the optimal number of clusters can thus be defined afterwards. The  
390 structure of the clustering process is visualized in a dendrogram (Fig. S1) and is used to  
391 choose the number of clusters, although that choice does require some subjective judgment  
392 (see SI).

393

### 394 **Statistical Analysis**

395 For the comparison of the first and second half of the studies time-period (Fig. 3a) we test  
396 for significance by randomly picking blocks of 7 days of each season from the time-series  
397 which contains the cluster events. The length was chosen based on the mean event-length  
398 of all clusters during the whole period. The blocks are then shuffled between years and  
399 calendar slots creating artificial time-series, but the order within the blocks is maintained

400 (preserving the intra-seasonal auto-correlation of the original time-series). This way we  
401 create a new time-series from which we calculate the frequency difference of the two data  
402 halves. We do this 10,000 times and calculate the percentiles of the observed frequency  
403 difference.

404

#### 405 **Composite plots**

406 Before computing the temperature composites (Fig. 4), the data was detrended to prevent  
407 biases due to trends in the occurrence of the clusters. The significance of the composites is  
408 tested creating 10,000 artificial time-series by randomly picking and shuffling blocks of the  
409 original time-series (with a block-length of five days). For each newly created time-series we  
410 pick as many days as were used to form the composite but we also keep the start days and  
411 length of the identified events from the original time-series to account for a potential  
412 increase in auto-correlation during long-lasting cluster events. For the precursors we  
413 similarly composite (Fig. 8) but we neglect polar vortex data of the very first 30 days (i.e.  
414 01.01.1979-30.01.1979) since leading sea level pressure and  $v^*T^*$  values are not included in  
415 the reanalysis datasets. The composites are then formed over the days preceding the onset  
416 of the identified cluster event.

417

#### 418 **Coincidence analysis**

419 To assess the coincidence of cold events in Eurasia and weak polar vortex states, we define  
420 cold days as days when the mean temperature anomaly over the Eurasian sector is below a  
421 certain threshold; e.g. below  $-5^{\circ}\text{C}$ . Next we calculate the frequency of each cluster on cold

422 days and compare to the frequency of each cluster on all days. To test significance for the  
423 observed frequency of a specific cluster  $i$ , we apply a chi-square test to the contingency table  
424 containing the cluster number (occurrence of cluster  $i$ / other than cluster  $i$ ) and the extreme  
425 event (occurrence of cold extreme/no cold extreme).

426 For the coincidence of anomalous sea level pressure over western Siberia and weak polar  
427 vortex states, we calculate a baseline (i.e. climatological) frequency for each cluster based on  
428 the 25-35 days following every day in December and January (neglecting December 1978  
429 which is not included) which coincides with the absolute frequencies of the different clusters  
430 as shown in Fig. 1. We compare that to the frequency for each cluster based on the 15 to 35  
431 day periods following Siberian High events. To assess the significance, we create 1000  
432 synthetic time series with the same number of Siberian High events as in observations, but  
433 randomly distributed in time. This way we get a distribution of the cluster events frequencies  
434 following Siberian High events and can calculate percentiles to get the corresponding P-  
435 value.

## 436 References

- 437 Baldwin, M. P., and D. O’Sullivan, 1995: Stratospheric Effects of ENSO-Related Tropospheric  
 438 Circulation Anomalies. *J. Clim.*, **8**, 649–667, doi:10.1175/1520-  
 439 0442(1995)008<0649:SEOERT>2.0.CO;2.
- 440 —, and T. J. Dunkerton, 1999: Propagation of the Arctic Oscillation from the stratosphere  
 441 to the troposphere. *J. Geophys. Res.*, **104**, 30937, doi:10.1029/1999JD900445.
- 442 Baldwin, M. P., and T. J. Dunkerton, 2001: Stratospheric harbingers of anomalous weather  
 443 regimes. *Science*, **294**, 581–584, doi:10.1126/science.1063315.
- 444 Butler, A. H., L. M. Polvani, and C. Deser, 2014: Separating the stratospheric and  
 445 tropospheric pathways of El Niño–Southern Oscillation teleconnections. *Environ. Res.*  
 446 *Lett.*, **9**, 24014, doi:10.1088/1748-9326/9/2/024014.
- 447 Butler, A. H., and Coauthors, 2015: Defining Sudden Stratospheric Warmings. *Bull. Am.*  
 448 *Meteorol. Soc.*, **96**, 1913–1928, doi:10.1175/BAMS-D-13-00173.1.
- 449 Charlton, A. J., and L. M. Polvani, 2007: A New Look at Stratospheric Sudden Warmings. Part  
 450 I: Climatology and Modeling Benchmarks. *J. Clim.*, **20**, 449–469, doi:10.1175/JCLI3996.1.
- 451 Cheng, X., and J. M. Wallace, 1993: Cluster Analysis of the Northern Hemisphere Wintertime  
 452 500-hPa Height Field: Spatial Patterns. *J. Atmos. Sci.*, **50**, 2674–2696, doi:10.1175/1520-  
 453 0469(1993)050<2674:CAOTNH>2.0.CO;2.
- 454 Cohen, J., 2016: An observational analysis: Tropical relative to Arctic influence on  
 455 midlatitude weather in the era of Arctic amplification. *Geophys. Res. Lett.*, **43**, 5287–  
 456 5294, doi:10.1002/2016GL069102.
- 457 —, and J. Jones, 2011: Tropospheric Precursors and Stratospheric Warmings. *J. Clim.*, **24**,  
 458 6562–6572, doi:10.1175/2011JCLI4160.1.
- 459 Cohen, J., J. Jones, J. C. Furtado, and E. Tziperman, 2013: Warm Arctic, Cold Continents.  
 460 *Oceanography*, **26**, 1–12.
- 461 Cohen, J., and Coauthors, 2014a: Recent Arctic amplification and extreme mid-latitude  
 462 weather. *Nat. Geosci.*, **7**, 627–637, doi:10.1038/ngeo2234.
- 463 —, J. C. Furtado, J. Jones, M. Barlow, D. Whittleston, and D. Entekhabi, 2014b: Linking  
 464 Siberian snow cover to precursors of stratospheric variability. *J. Clim.*, **27**, 5422–5432.
- 465 Dee, D. P., and Coauthors, 2011: The ERA-Interim reanalysis: configuration and performance  
 466 of the data assimilation system. *Q. J. R. Meteorol. Soc.*, **137**, 553–597,  
 467 doi:10.1002/qj.828.
- 468 Dunn-Sigouin, E., and T. A. Shaw, 2015: Comparing and contrasting extreme stratospheric

469 events, including their coupling to the tropospheric circulation. *J. Geophys. Res. Atmos.*,  
470 **120**, 1374–1390, doi:10.1002/2014JD022116.

471 Feldstein, S. B., and S. Lee, 2014: Intraseasonal and interdecadal jet shifts in the Northern  
472 Hemisphere: The role of warm pool tropical convection and sea ice. *J. Clim.*, **27**, 6497–  
473 6518, doi:10.1175/JCLI-D-14-00057.1.

474 Garfinkel, C. I., and D. L. Hartmann, 2008: Different ENSO teleconnections and their effects  
475 on the stratospheric polar vortex. *J. Geophys. Res.*, **113**, D18114,  
476 doi:10.1029/2008JD009920.

477 Garfinkel, C. I., S.-W. Son, K. Song, V. Aquila, and L. D. Oman, 2017: Stratospheric variability  
478 contributed to and sustained the recent hiatus in Eurasian winter warming. *Geophys.*  
479 *Res. Lett.*, **44**, 374–382, doi:10.1002/2016GL072035.

480 Handorf, D., R. Jaiser, K. Dethloff, A. Rinke, and J. Cohen, 2015: Impacts of Arctic sea-ice and  
481 continental snow-cover changes on atmospheric winter teleconnections. *Geophys. Res.*  
482 *Lett.*, **42**, n/a-n/a, doi:10.1002/2015GL063203.

483 Hitchcock, P., and I. R. Simpson, 2014: The Downward Influence of Stratospheric Sudden  
484 Warmings\*. *J. Atmos. Sci.*, **71**, 3856–3876, doi:10.1175/JAS-D-14-0012.1.

485 —, and Coauthors, 2013a: Lower-Stratospheric Radiative Damping and Polar-Night Jet  
486 Oscillation Events. *J. Atmos. Sci.*, **70**, 1391–1408, doi:10.1175/JAS-D-12-0193.1.

487 —, T. G. Shepherd, and G. L. Manney, 2013b: Statistical Characterization of Arctic Polar-  
488 Night Jet Oscillation Events. *J. Clim.*, **26**, 2096–2116, doi:10.1175/JCLI-D-12-00202.1.

489 Horton, D. E., N. C. Johnson, D. Singh, D. L. Swain, B. Rajaratnam, and N. S. Diffenbaugh,  
490 2015: Contribution of changes in atmospheric circulation patterns to extreme  
491 temperature trends. *Nature*, **522**, 465–469, doi:10.1038/nature14550.

492 Jaiser, R., K. Dethloff, and D. Handorf, 2013: Stratospheric response to Arctic sea ice retreat  
493 and associated planetary wave propagation changes. *Tellus A*, **65**,  
494 doi:10.3402/tellusa.v65i0.19375.

495 —, T. Nakamura, D. Handorf, K. Dethloff, J. Ukita, and K. Yamazaki, 2016: Atmospheric  
496 winter response to Arctic sea ice changes in reanalysis data and model simulations. *J.*  
497 *Geophys. Res. Atmos.*, doi:10.1002/2015JD024679.

498 Kim, B.-M., S.-W. Son, S.-K. Min, J.-H. Jeong, S.-J. Kim, X. Zhang, T. Shim, and J.-H. Yoon, 2014:  
499 Weakening of the stratospheric polar vortex by Arctic sea-ice loss. *Nat. Commun.*, **5**,  
500 4646, doi:10.1038/ncomms5646.

501 Kodera, K., H. Mukougawa, P. Maury, M. Ueda, and C. Claud, 2016: Absorbing and reflecting  
502 sudden stratospheric warming events and their relationship with tropospheric  
503 circulation. *J. Geophys. Res. Atmos.*, **121**, 80–94, doi:10.1002/2015JD023359.

504 Kolstad, E. W., T. Breiteig, and A. A. Scaife, 2010: The association between stratospheric



- 505 weak polar vortex events and cold air outbreaks in the Northern Hemisphere. *Q. J. R.*  
506 *Meteorol. Soc.*, **136**, 886–893, doi:10.1002/qj.620.
- 507 Kretschmer, M., D. Coumou, J. F. Donges, and J. Runge, 2016: Using Causal Effect Networks  
508 to analyze different Arctic drivers of mid-latitude winter circulation. *J. Clim.*, 4069–4081,  
509 doi:10.1175/JCLI-D-15-0654.1.
- 510 Lee, S., and S. B. Feldstein, 2013: Detecting ozone- and greenhouse gas-driven wind trends  
511 with observational data. *Science*, **339**, 563–567, doi:10.1126/science.1225154.
- 512 Li, C., B. Stevens, and J. Marotzke, 2015: Eurasian winter cooling in the warming hiatus of  
513 1998–2012. *Geophys. Res. Lett.*, **42**, 8131–8139, doi:10.1002/2015GL065327.
- 514 Matsuno, T., 1970: Vertical Propagation of Stationary Planetary Waves in the Winter  
515 Northern Hemisphere. *J. Atmos. Sci.*, **27**, 871–883, doi:10.1175/1520-  
516 0469(1970)027<0871:VPOSPW>2.0.CO;2.
- 517 McCusker, K. E., J. C. Fyfe, and M. Sigmond, 2016: Twenty-five winters of unexpected  
518 Eurasian cooling unlikely due to Arctic sea-ice loss. *Nat. Geosci.*, **9**, 838–842,  
519 doi:10.1038/ngeo2820.
- 520 Molod, A., L. Takacs, M. Suarez, and J. Bacmeister, 2015: Development of the GEOS-5  
521 atmospheric general circulation model: evolution from MERRA to MERRA2. *Geosci.*  
522 *Model Dev.*, **8**, 1339–1356, doi:10.5194/gmd-8-1339-2015.
- 523 Mori, M., M. Watanabe, H. Shiogama, J. Inoue, and M. Kimoto, 2014: Robust Arctic sea-ice  
524 influence on the frequent Eurasian cold winters in past decades. *Nat. Geosci.*, **7**, 869–  
525 873, doi:10.1038/ngeo2277.
- 526 Overland, J. E., K. R. Wood, and M. Wang, 2011: Warm Arctic—cold continents: climate  
527 impacts of the newly open Arctic Sea. *Polar Res.*, **30**, doi:10.3402/polar.v30i0.15787.
- 528 —, and Coauthors, 2016: Nonlinear response of mid-latitude weather to the changing  
529 Arctic. *Nat. Clim. Chang.*, **6**, 992–999, doi:10.1038/nclimate3121.
- 530 Palmer, T., 2014: Record-breaking winters and global climate change. *Science (80-. )*, **344**,  
531 803–804.
- 532 Polvani, L. M., and D. W. Waugh, 2004: Upward Wave Activity Flux as a Precursor to Extreme  
533 Stratospheric Events and Subsequent Anomalous Surface Weather Regimes. *J. Clim.*, **17**,  
534 3548–3554, doi:10.1175/1520-0442(2004)017<3548:UWAFAA>2.0.CO;2.
- 535 —, and Coauthors, 2016: Distinguishing stratospheric sudden warmings from ENSO as key  
536 drivers of wintertime climate variability over the North Atlantic and Eurasia. *J. Clim.*,  
537 JCLI-D-16-0277.1, doi:10.1175/JCLI-D-16-0277.1.
- 538 Runde, T., M. Dameris, H. Garny, and D. E. Kinnison, 2016: Classification of stratospheric  
539 extreme events according to their downward propagation to the troposphere. *Geophys.*  
540 *Res. Lett.*, **43**, 6665–6672, doi:10.1002/2016GL069569.

- 541 Scaife, A. A., and Coauthors, 2016: Seasonal winter forecasts and the stratosphere. *Atmos.*  
542 *Sci. Lett.*, **17**, 51–56, doi:10.1002/asl.598.
- 543 Screen, J. A., and I. Simmonds, 2010: The central role of diminishing sea ice in recent Arctic  
544 temperature amplification. *Nature*, **464**, 1334–1337, doi:10.1038/nature09051.
- 545 —, and J. A. Francis, 2016: Contribution of sea-ice loss to Arctic amplification is regulated  
546 by Pacific Ocean decadal variability. *Nat. Clim. Chang.*, **6**, 856–860,  
547 doi:10.1038/nclimate3011.
- 548 Shaw, T. A., J. Perlwitz, and O. Weiner, 2014: Troposphere-stratosphere coupling: Links to  
549 North Atlantic weather and climate, including their representation in CMIP5 models. *J.*  
550 *Geophys. Res. Atmos.*, **119**, 5864–5880, doi:10.1002/2013JD021191.
- 551 Shepherd, T. G., 2016: Effects of a warming Arctic. *Science (80-. )*, **353**.
- 552 Sigmond, M., J. F. Scinocca, V. V. Kharin, and T. G. Shepherd, 2013: Enhanced seasonal  
553 forecast skill following stratospheric sudden warmings. *Nat. Geosci.*, **6**, 98–102,  
554 doi:10.1038/ngeo1698.
- 555 Smith, K. L., C. G. Fletcher, P. J. Kushner, K. L. Smith, C. G. Fletcher, and P. J. Kushner, 2010:  
556 The Role of Linear Interference in the Annular Mode Response to Extratropical Surface  
557 Forcing. *J. Clim.*, **23**, 6036–6050, doi:10.1175/2010JCLI3606.1.
- 558 Sun, L., C. Deser, and R. A. Tomas, 2015: Mechanisms of Stratospheric and Tropospheric  
559 Circulation Response to Projected Arctic Sea Ice Loss\*. *J. Clim.*, **28**, 7824–7845,  
560 doi:10.1175/JCLI-D-15-0169.1.
- 561 —, J. Perlwitz, and M. Hoerling, 2016: What caused the recent “Warm Arctic, Cold  
562 Continents” trend pattern in winter temperatures? *Geophys. Res. Lett.*, **43**, 5345–5352,  
563 doi:10.1002/2016GL069024.

564

565

## 566 **Figure Captions List**

### 567 **Figure 1:**

568 *Polar vortex clusters and their frequency trends. Composite mean of 10hPa geopotential*  
569 *heights values over all days that were assigned to the same cluster (clustering performed*  
570 *with zonal wind anomalies) and time series of normalized occurrence frequency in winter (JF)*  
571 *with least-square fit line. The number in parentheses denotes the total frequency occurrence*  
572 *(in percent) for the studied period.*

573

### 574 **Figure 2:**

575 *Trend in strongest and weakest polar vortex clusters explain the overall trend of the polar*  
576 *vortex. a) Seasonal-mean (JF) trend in zonal wind poleward of 40°N. Significant values*  
577 *( $P < 0.1$ ) according to two-sided Student's t-test are shown in hatches. b) Sum of all seven*  
578 *polar vortex cluster representatives multiplied by their trend in seasonal frequency. c) Same*  
579 *as b) but only for cluster 1 and 7.*

580

### 581 **Figure 3:**

582 *Average occurrence (in days) per winter of each cluster from 1979-1996 (light blue) and from*  
583 *1998-2015 (dark blue) and the change in percent. Significant changes ( $P < 0.05$ ) are indicated*  
584 *in red.*

585

586 **Figure 4:**

587 *Composites of detrended near-surface temperature during a) cluster 1 and b) cluster 7 days.*

588 *Significant values ( $P < 0.05$ ) are indicated with dots.*

589

590 **Figure 5:**

591 *Explained variance ( $R^2$  values) of winter (JF) mean temperature for regression with a) winter*  
592 *mean Nino3.4 index , b) winter mean polar cap height (PCH), c) cluster 7 frequency, d) cluster*  
593 *7 frequency and the winter mean Nino3.4 index. Before calculation the regression models,*  
594 *the linear trends of the regressors and the temperature was removed. Significant ( $P < 0.05$ )*  
595 *models according to F-test are indicated in hatches.*

596

597 **Figure 6:**

598 *a)-c) Linear trends in temperature as projected by the regression models in Figure 5a,c,d and*  
599 *d) observed trends for the period 1990-2015. The regression models were calculated based on*  
600 *detrended data from 1979-2015 and the projected trends are calculated for the undetrended*  
601 *regressors from 1990-2015.*

602

603 **Figure 7:**

604 *Coincidence analysis for extreme cold days over a) the Eurasian sector ( $15^{\circ}$ - $130^{\circ}$ E,  $50^{\circ}$ - $65^{\circ}$ N).*

605 *b) The deviation from the statistically expected occurrence frequency (as displayed in Figure*  
606 *1) of each cluster is shown during cold days ( $<-5^{\circ}\text{C}$ ).*

607

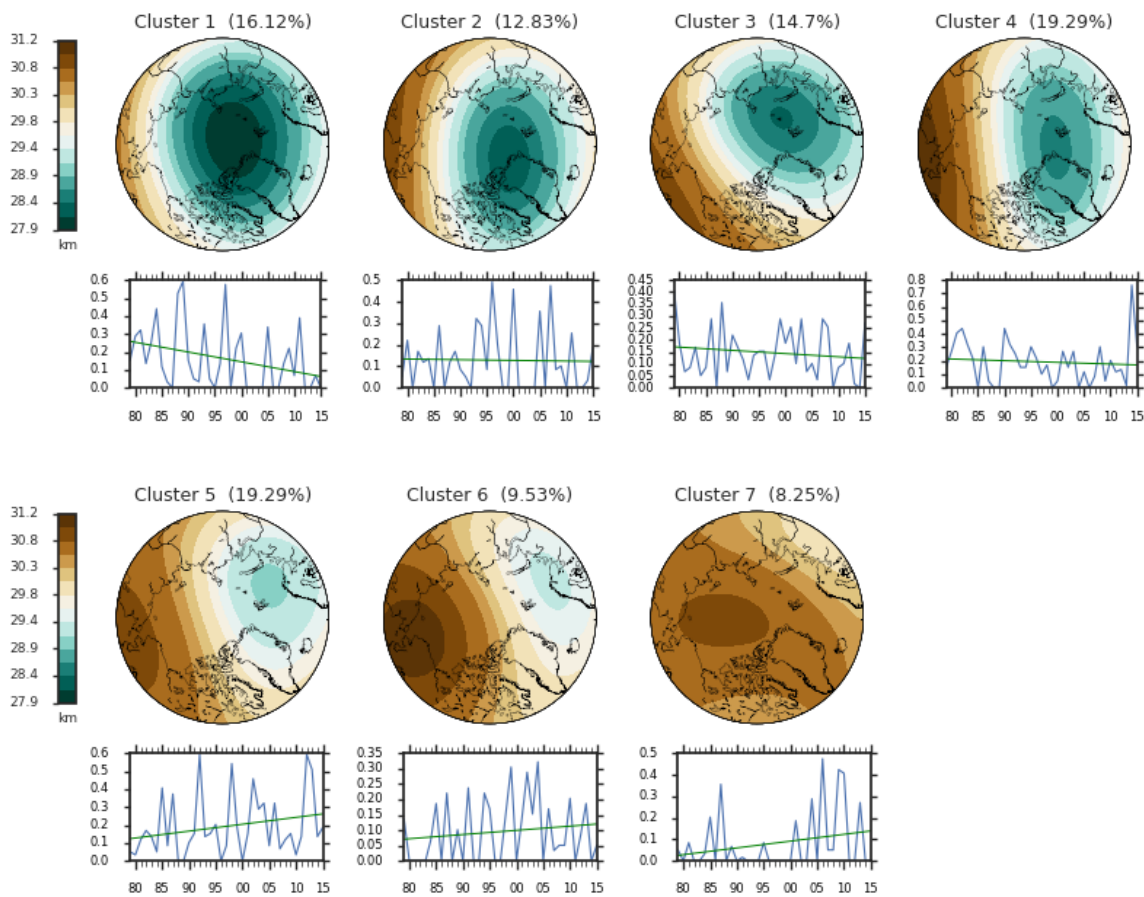
608 **Figure 8:**

609 *Precursors to cluster events. Composite of (detrended) sea level pressure anomalies 30-10*  
610 *days prior to start days of a) cluster 1 and b) cluster 7 events. c), d) as a), b) but for*  
611 *(detrended) poleward heat-flux  $v^*T^*$  anomalies at 100hPa averaged 10 days before onset of*  
612 *cluster event. In all panels, significant values ( $P<0.05$ ) are indicated with dots.*

613

614 **Figures**

615 **Figure 1:**

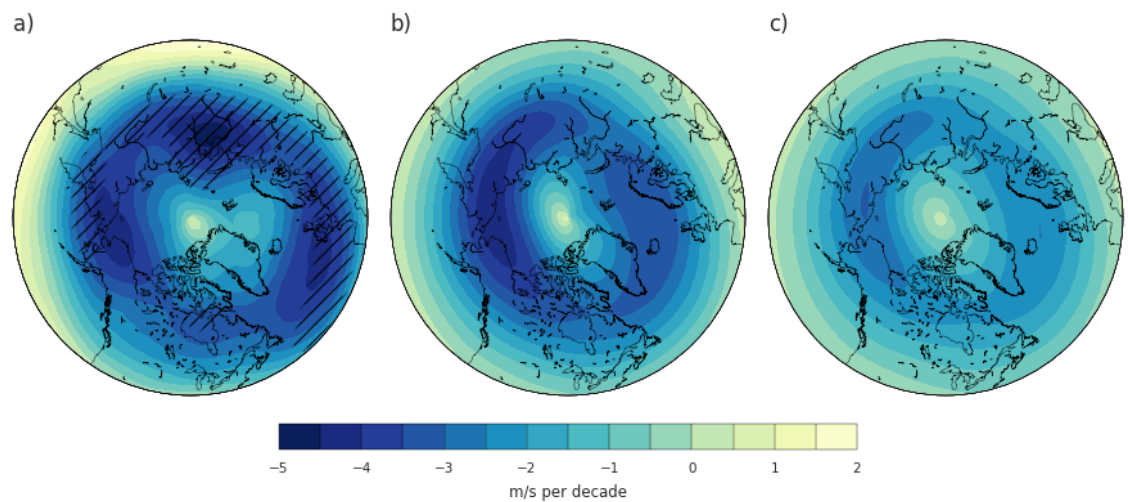


616

617 *Polar vortex clusters and their frequency trends. Composite mean of 10hPa geopotential*  
618 *heights values over all days that were assigned to the same cluster (clustering performed*  
619 *with zonal wind anomalies) and time series of normalized occurrence frequency in winter (JF)*  
620 *with least-square fit line. The number in parentheses denotes the total frequency occurrence*  
621 *(in percent) for the studied period.*

622

623 **Figure 2:**



624

625 *Trend in strongest and weakest polar vortex clusters explain the overall trend of the polar*  
626 *vortex. a) Seasonal-mean (JF) trend in zonal wind poleward of 40°N. Significant values*  
627 *( $P < 0.1$ ) according to two-sided Student's t-test are shown in hatches. b) Sum of all seven*  
628 *polar vortex cluster representatives multiplied by their trend in seasonal frequency. c) Same*  
629 *as b) but only for cluster 1 and 7.*

630

631 **Figure 3:**



632

633 Average occurrence (in days) per winter of each cluster from 1979-1996 (light blue) and from

634 1998-2015 (dark blue) and the change in percent. Significant changes ( $P < 0.05$ ) are indicated

635 in red.

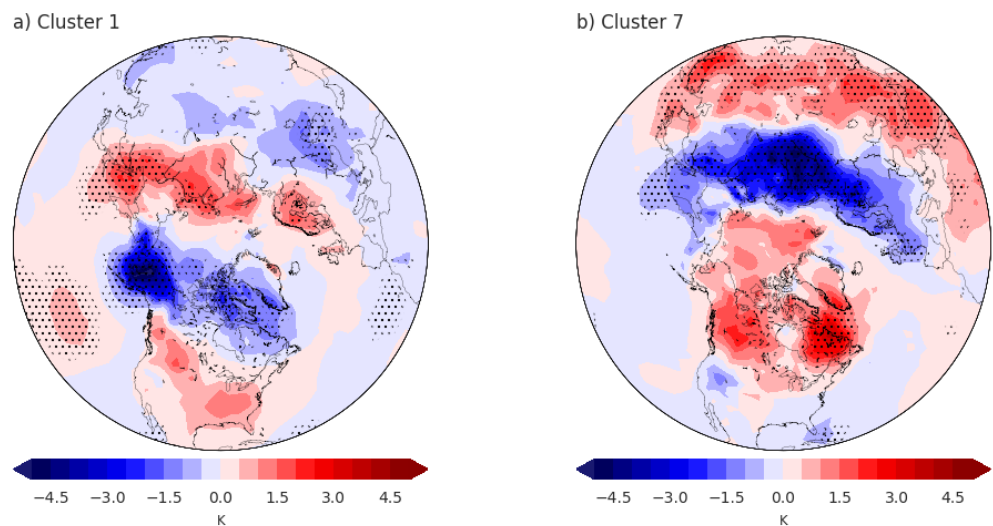
636

637



638 **Figure 4:**

639

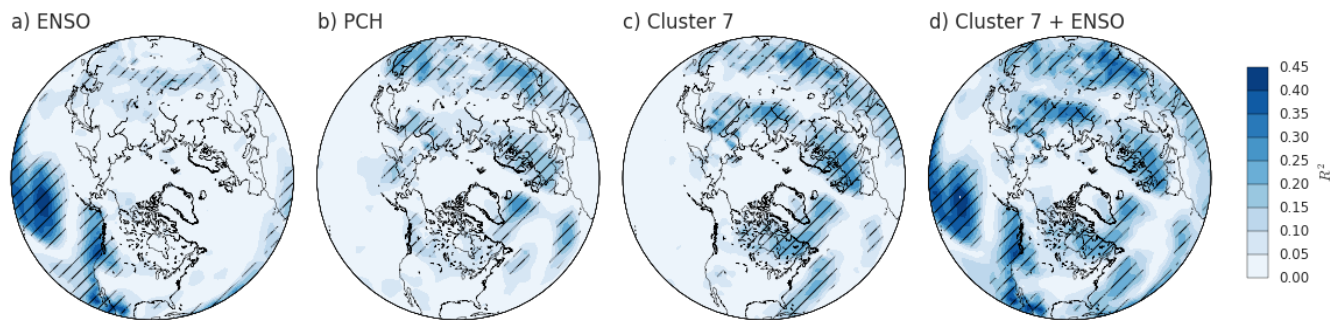


641 *Composites of detrended near-surface temperature during a) cluster 1 and b) cluster 7 days.*

642 *Significant values ( $P < 0.05$ ) are indicated with dots.*

643

644 **Figure 5:**

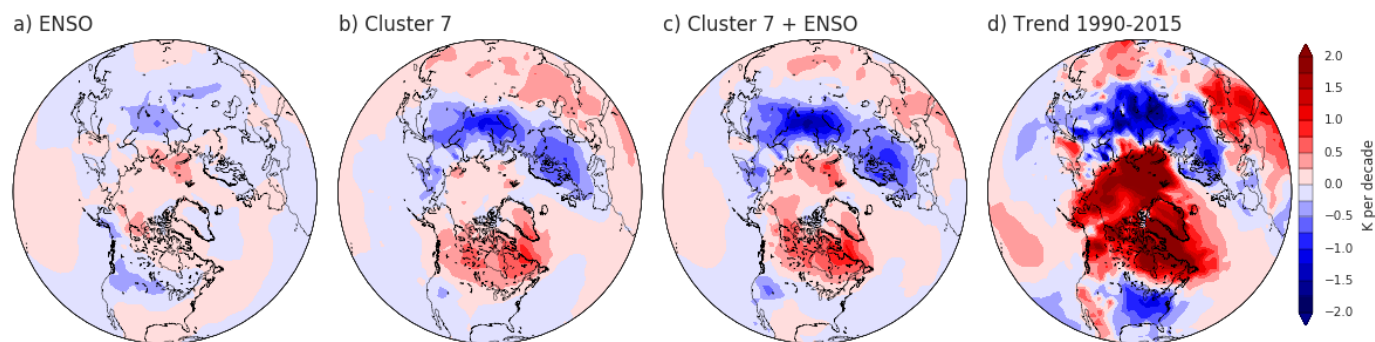


645

646 *Explained variance ( $R^2$  values) of winter (JF) mean temperature for regression with a) winter*  
647 *mean Nino3.4 index , b) winter mean polar cap height (PCH), c) cluster 7 frequency, d) cluster*  
648 *7 frequency and the winter mean Nino3.4 index. Before calculation the regression models,*  
649 *the linear trends of the regressors and the temperature was removed. Significant ( $P < 0.05$ )*  
650 *models according to F-test are indicated in hatches.*

651

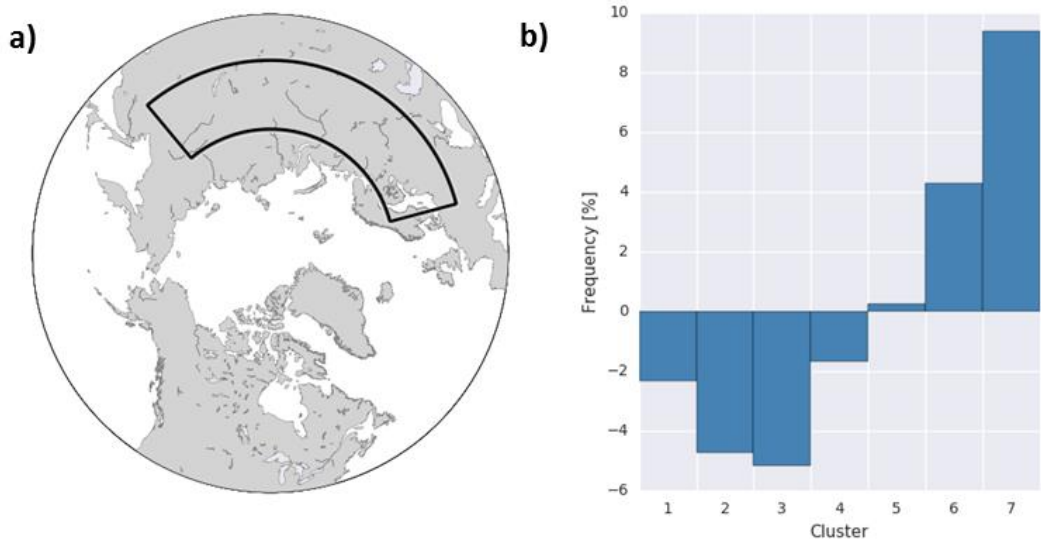
652 **Figure 6:**



653

654 *a)-c) Linear trends in temperature as projected by the regression models in Figure 5a,c,d and*  
655 *d) observed trends for the period 1990-2015. The regression models were calculated based on*  
656 *detrended data from 1979-2015 and the projected trends are calculated for the undetrended*  
657 *regressors from 1990-2015.*

658 **Figure 7:**



659

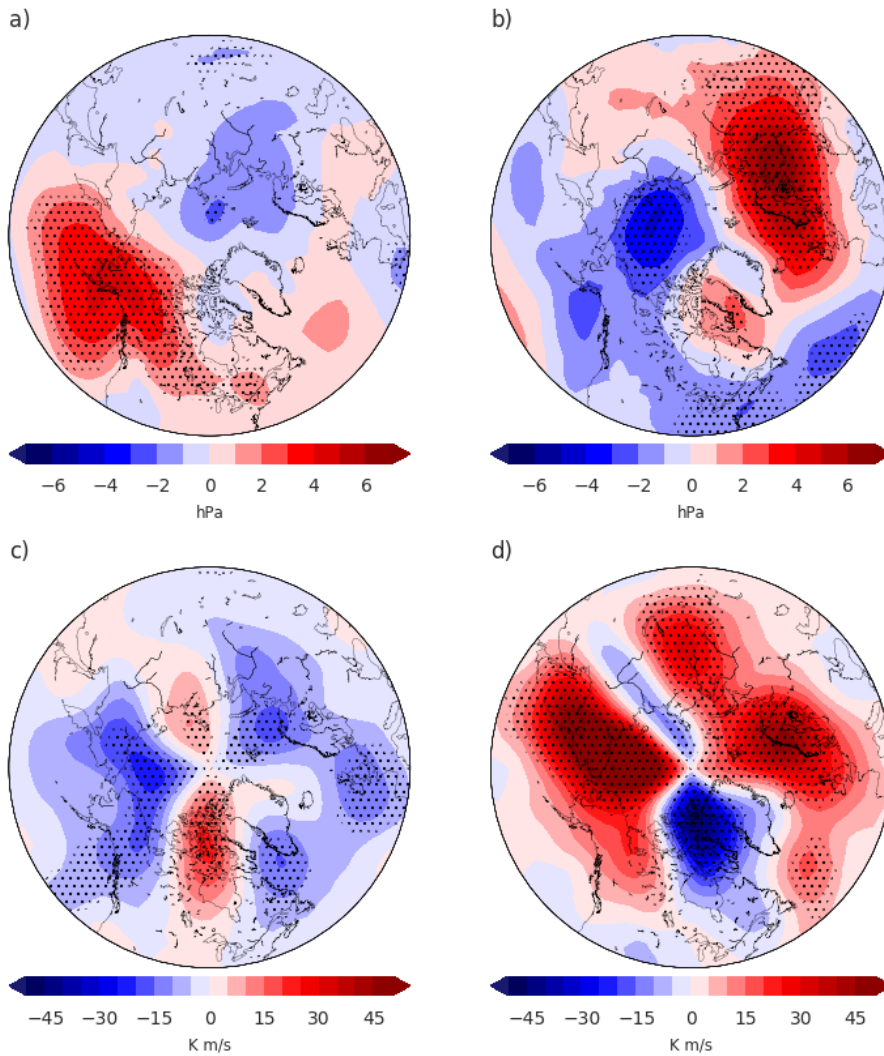
660 *Coincidence analysis for extreme cold days over a) the Eurasian sector (15°-130°E, 50°-65°N).*

661 *b) The deviation from the statistically expected frequency (as displayed in Figure 1) of each*

662 *cluster is shown during cold days (<-5°C).*

663

664 **Figure 8:**



665

666 *Precursors to cluster events. Composite of (detrended) sea level pressure anomalies 30-10*  
 667 *days prior to start days of a) cluster 1 and b) cluster 7 events. c), d) as a), b) but for*  
 668 *(detrended) poleward heat-flux  $v \cdot T^*$  anomalies at 100hPa averaged 10 days before onset of*  
 669 *cluster event. In all panels, significant values ( $P < 0.05$ ) are indicated with dots.*